Inertial Sensor Based Indoor Localization and Monitoring System for Emergency Responders

Rui Zhang, Fabian Höflinger, and Leonhard Reindl, *Member, IEEE*

***Abstract*— This paper presents a novel indoor localization and monitoring system based on inertial sensors for emergency responders. The system utilizes acceleration, angular rate and magnetic field sensors and consists of three parts. The first part is a modified Kalman filtering which implements the sensor data fusion and meanwhile detects and minimizes the magnetic field disturbances, so as to provide a long term stable orientation solution. The second part is zero velocity updating which resets the velocity within still phase to deliver accurate position information. The last part of the system is body movement monitoring, which is achieved by calculating the relative position of each body segment based on the transformation of coordinate frame of each body segment. The experimental result shows that the system is able to track person indoors in both walking and running cases, and to monitor the body movement during whole period of experiment.**

***Index Terms*— Indoor localization, inertial measurement unit (IMU), Kalam filter, magnetic field disturbances, orientation, sensor data fusion, zero velocity update (ZUPT).**

I. Introduction

AS PART of the German research project I-LOV[1] aiming at improving urban search and rescue, the work presented in this paper is to localize rescue crew and monitor the behavior of the rescue crew, in order to minimize the personnel loss and enhance the security of the mission. Since in most cases the responders operate inside the buildings and GPS signal can be blocked by buildings, a non-GPS localization technology is necessary.

Normally non-GPS approaches for personal positioning require external references [1]. Zhang used wireless infrastructure to track moving objects by applying interacting multiple mode algorithm with time of arrival measurements [2], [3]. Sippel used optical laser tracking system consisting of a laser base station and a intelligent sensor node to obtain the information of position [4]. Generally, these reference-based systems have advantages of being able to deliver absolute position and orientation in real-time so that the error will not grow with time. However, these systems can only be utilized if the application permits the installation of those external references ahead of time.

Inertial sensor based localization using inertial sensors such as accelerometers and gyroscopes requires no external references and no installation beforehand, since those sensors do not depend on the environment where responders are located and have been embedded in the clothes and shoes of the responders beforehand. However, due to the sensor drift and recursive calculation, the orientation error will grow with time. Incorrect orientation will affect the determined accuracy of position, since accurate orientation information is the precondition for personal tracking/positioning and movement monitoring. In order to provide a long term stable orientation solution, magnetic field sensor is fused with inertial sensors by Kalman filter.

There are many methods to design Kalman filter based sensor data fusion. The straight forward method presented in [5] is to set the gyro based orientation data as state-estimate, gravity and magnetic field based orientation as the measurement to correct the predicted state-estimate. When using this method, the dynamic system model must be derived. Unfortunately, human motion is very difficult to model and predict even with large computational consumption. Based on Foxlin's method an error state, separated bias Kalman filter-based data fusion was applied in [6]–[8], which avoided modeling the body angles motion and its interaction with the environment. However, as this method did not mention how to handle magnetic field disturbances, the sensed data could be significantly polluted. In literature [9]–[11] the Kalman filter structure designed by Roetenberg and Luinge was able to compensate the magnetic field disturbances by using predefined sensor model for magnetic field sensor. The parameter of the sensor model was obtained by characterizing the disturbances by moving the sensor at different speeds and distances from the ferromagnetic materials. However, there was no further detail about how to determine the parameters of the model. Foxlin and Jiménez came up with an idea to include the velocity and position error inside the filter, which efficiently reduced the drift error of inertial sensors, and produced a possible solution without magnetic sensor [12]–[14]. However, in order to achieve higher tracking accuracy, the magnetic sensor is necessary. But we found that the result was much worse with magnetic sensor than the one without magnetic sensor, when local magnetic field was contaminated. Besides, incorrect position and velocity data could also affect the orientation calculation. Calusdian and Yun presented a simple idea to fuse

Manuscript received July 19, 2012; accepted October 23, 2012. Date of publication November 15, 2012; date of current version January 15, 2013. This work was supported by the German Federal Ministry of Education and Research under Grant 13N9759. The associate editor coordinating the review of this paper and approving it for publication was Dr. Kailash Thakur.

The authors are with the Department of Microsystems Engineering, University of Freiburg, Freiburg 79110, Germany (e-mail: rui.zhang@imtek.uni-freiburg.de; Fabian.Hoeflinger@imtek.de; reindl@imtek.uni-freiburg.de).

Color versions of one or more of the figures in this paper are available online at http://ieeexplore.ieee.org.

Digital Object Identifier 10.1109/JSEN.2012.2227593

[1]**I**ntelligentes, sicherndes **Lo**kalisierungssystem für die Rettung und Bergung **V**erschütteter in English "intelligent, securing locating system for the rescue and extraction of trapped victims"

the orientation information based on quaternion by utilizing a gain factor to handle the static and dynamic cases [15], [16]. However, the method worked only when the magnetic field was nearly homogeneous with fewer disturbances. To solve this problem, earlier we presented an work which added a function for detecting and minimizing the magnetic field disturbance to the complementary separate-bias Kalman filter so as to handle the magnetic sensor data appropriately [17].

Unfortunately, even if accurate orientation information has been obtained, large velocity and position errors were still found after two times integrations of acceleration due to sensor drift. This problem can be solved using zero velocity update (ZUPT) method to reset the foot speed of each step [18], [19]. This idea has also been successfully implemented in several studies [12]–[16] and [20].

In order to give on time first-aid medical treatment or equipment supply, real-time human body monitoring is required. Renaudin presented a distributed architecture of sensor modules for agent, in which chest-attached sensor module was used for orientation analysis, both thigh- and chest-attached sensor modules were used for posture analysis and leg-attached sensor module was used for gait analysis [21]. Zhou and Hu presented an inertial sensor based monitoring system for measuring the movement of human upper limbs [22]. Zhu and Zhou described a real-time motion tracking system, which required more than ten sensor modules for whole body kinematics analysis [23]. Adapted from the last method, in this study the orientation information instead of the gravity and magnetic field information of each human body segment is used to achieve the relative position of each segment.

The reminder of this paper is structured as follows. In section II modified Kalman filter with two functions for magnetic field disturbances solution is presented. In section III ZUPT method is presented. Section VI shows the kinematic monitoring of human movement by using accurate orientation information. The experiment results and discussion are presented in section V. Conclusion and future work are given in section VI.

II. Orientation Determination

The following subsections will demonstrate two main functions of the modified complementary Kalman filter: the complementary separate-bias Kalman filtering for data fusion without motion modeling; the magnetic disturbances detection and minimization for improvement of system's robustness and stability when experiencing local magnetic field disturbances.

A. Complementary Kalman Filter

The orientation of the inertial sensor module which is also called IMU with respect to a Body-fixed frame of axes noted as **b**-frame of time step k is defined by three Euler angles: $\Phi_k = [\varphi,\ \theta,\ \psi]$ as roll, pitch and yaw angle, which are shown in Fig. 1. The Euler angles can be derived by using angular rate in **b**-frame: $\boldsymbol{\Omega}_{b,k} = [\omega_x,\ \omega_y,\ \omega_z]^T$ and a set of known Euler angles at a given time as initial orientation. However, since $\tan\theta$ tends to infinity for pitch angles around $\pm 90°$, the error becomes unbounded. In order to overcome this problem,

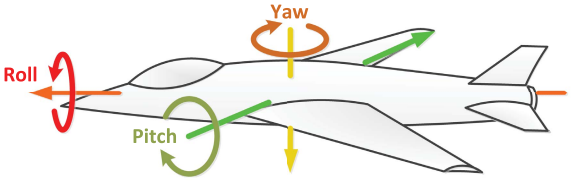

Fig. 1. Orientation represented by Euler angles.

quaternion algebra is used to present orientation with Euler parameters $\mathbf{q}_k = [e_0,\ e_1,\ e_2,\ e_3]^T$ instead of Euler angles.

The procedures to calculate inertial sensor based orientation, velocity and position is shown as follows:

1) Use Euler parameters to present the initial orientation instead of Euler angles. The initial orientation is obtained by magnetic field sensor and acceleration sensor, which will be given later on.

$$e_0 = \cos\frac{\psi}{2}\cos\frac{\theta}{2}\cos\frac{\varphi}{2} + \sin\frac{\psi}{2}\sin\frac{\theta}{2}\sin\frac{\varphi}{2} \tag{1}$$

$$e_1 = \cos\frac{\psi}{2}\cos\frac{\theta}{2}\sin\frac{\varphi}{2} - \sin\frac{\psi}{2}\sin\frac{\theta}{2}\cos\frac{\varphi}{2} \tag{2}$$

$$e_2 = \cos\frac{\psi}{2}\sin\frac{\theta}{2}\sin\frac{\varphi}{2} + \sin\frac{\psi}{2}\cos\frac{\theta}{2}\sin\frac{\varphi}{2} \tag{3}$$

$$e_3 = -\cos\frac{\psi}{2}\sin\frac{\theta}{2}\sin\frac{\varphi}{2} + \sin\frac{\psi}{2}\cos\frac{\theta}{2}\cos\frac{\varphi}{2} \tag{4}$$

2) Calculate the change of Euler parameter $\dot{\mathbf{q}}_k = [\dot{e}_0,\ \dot{e}_1,\ \dot{e}_2,\ \dot{e}_3]^T$ using angular rate data $\boldsymbol{\Omega}_{b,k}$ from gyroscopes.

$$\dot{e}_0 = -\frac{1}{2}(e_1\omega_x + e_2\omega_y + e_3\omega_z) \tag{5}$$

$$\dot{e}_1 = \frac{1}{2}(e_0\omega_x + e_2\omega_z - e_3\omega_y) \tag{6}$$

$$\dot{e}_2 = \frac{1}{2}(e_0\omega_y + e_3\omega_x - e_1\omega_z) \tag{7}$$

$$\dot{e}_3 = \frac{1}{2}(e_0\omega_z + e_1\omega_y - e_2\omega_x) \tag{8}$$

3) Integrate to Euler parameters at current time step with time duration dt.

$$\mathbf{q}_k = \mathbf{q}_{k-1} + \dot{\mathbf{q}}_k \cdot dt \tag{9}$$

4) Normalize the norm value of Euler parameters to 1 at all points of time.

$$e_0^2 + e_1^2 + e_2^2 + e_3^2 = 1 \tag{10}$$

5) Transform Euler parameters back to Euler angles for velocity and position integration.

$$\theta = sin^{-1}[-2(e_1e_3 - e_0e_2)] \tag{11}$$

$$\varphi = \arccos\left[\frac{e_0^2 - e_1^2 - e_2^2 + e_3^2}{\sqrt{1 - 4(e_1e_3 - e_0e_2)^2}}\right] \times \mathrm{sgn}[2(e_2e_3 + e_0e_1)] \tag{12}$$

$$\psi = \arccos\left[\frac{e_0^2 + e_1^2 - e_2^2 - e_3^2}{\sqrt{1 - 4(e_1e_3 - e_0e_2)^2}}\right] \times \mathrm{sgn}[2(e_1e_2 + e_0e_3)] \tag{13}$$

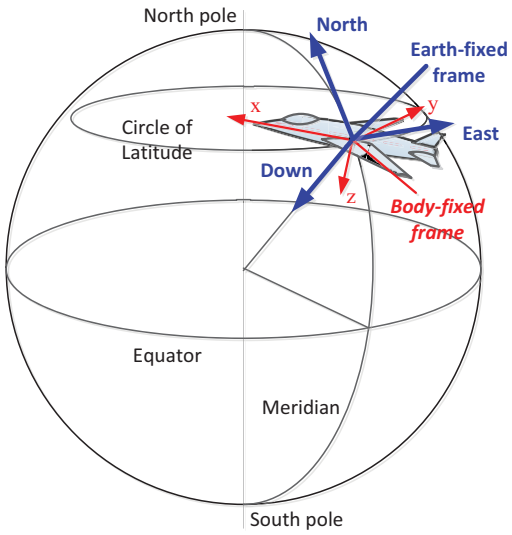

Fig. 2. Body- and Earth-fixed frames [24].

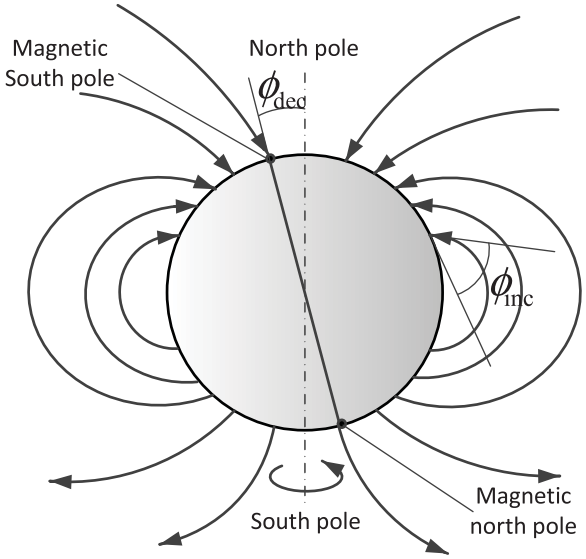

Fig. 3. Geomagnetic field [26].

6) Calculate the Direction Cosine Matrix (**DCM**) which transforms sensor data from **b**-frame into Earth-fixed frame noted as **n**-frame. Both frames are shown in Fig. 2.

$$\mathbf{DCM} = [D_1,\ D_2,\ D_3] \tag{14}$$

$$D_1 = \begin{bmatrix} \cos\theta\cos\psi \\ \sin\theta\sin\varphi\cos\psi - \sin\psi\cos\varphi \\ \sin\theta\cos\varphi\cos\psi + \sin\psi\sin\varphi \end{bmatrix} \tag{15}$$

$$D_2 = \begin{bmatrix} \cos\theta\sin\psi \\ \sin\psi\sin\theta\cos\varphi + \cos\psi\cos\varphi \\ \sin\psi\sin\theta\cos\varphi - \cos\psi\sin\theta \end{bmatrix} \tag{16}$$

$$D_3 = \begin{bmatrix} -\sin\theta \\ \sin\varphi + \cos\theta \\ \cos\varphi\cos\theta \end{bmatrix} \tag{17}$$

7) Calculate velocity and position in **n**-frame $\mathbf{V}_{n,k} = [v_x,\ v_y,\ v_z]^T$, $\mathbf{P}_{n,k} = [X,\ Y,\ Z]^T$ by taking the first and second integral of acceleration in **n**-frame $\mathbf{A}_{n,k}$ with respect to dt. However, since acceleration sensor output $\mathbf{A}_{b,k} = [a_x,\ a_y,\ a_z]^T$ contains the component of gravity, the acceleration due to the movement must be extracted.

$$\mathbf{A}_{n,k} = \mathbf{DCM} \cdot \mathbf{A}_{b,k} - [0,\ 0,\ g]^T, \tag{18}$$

where the gravity $g = 9.81$ m^2/s.

$$\mathbf{V}_{n,k} = \mathbf{V}_{n,k-1} + \mathbf{A}_{n,k} \cdot dt \tag{19}$$

$$\mathbf{P}_{n,k} = \mathbf{P}_{n,k-1} + \mathbf{V}_{n,k} \cdot dt \tag{20}$$

8) Repeat step 2 to 7 for all the time steps.

Since gyro based orientation is calculated iteratively, the sensor drift error will be accumulated. In order to compensate for this error, acceleration and magnetic field sensors are used to provide an instant reference orientation $\Phi^{\mathrm{R}} = [\varphi^{\mathrm{R}},\ \theta^{\mathrm{R}},\ \psi^{\mathrm{R}}]$. For static case, $\mathbf{A}_{n,k} \approx [0,\ 0,\ g]^T$ and $\mathbf{A}_{b,k}$ will only have gravity components in **b**-frame. Hence, the reference roll and pitch angles can be determined as follows:

$$\theta^{\mathrm{R}} = \arcsin\left(\frac{a_x}{-g}\right) \tag{21}$$

$$\varphi^{\mathrm{R}} = \arcsin\left(\frac{a_y}{a_z}\right) \tag{22}$$

The reference yaw angle is determined using magnetic field sensor, which provides data regarding to the earth's magnetic field on three orthogonal axes in **b**-frame, called the magnetic field vector $\mathbf{M}_{b,k} = [m_{b,x},\ m_{b,y},\ m_{b,z}]^T$. The horizontal components of magnetic field in the **n**-frame, X_h and Y_h, are expressed as:

$$X_h = m_{b,x}\cos\theta^{\mathrm{R}} + m_{b,y}\sin\varphi^{\mathrm{R}}\sin\theta^{\mathrm{R}} - m_{b,z}\cos\varphi^{\mathrm{R}}\sin\theta^{\mathrm{R}} \tag{23}$$

$$Y_h = m_{b,x}\cos\varphi^{\mathrm{R}} + m_{b,z}\sin\varphi^{\mathrm{R}} \tag{24}$$

Then the yaw angle is calculated by

$$\psi^{\mathrm{R}} = -\arctan\left(\frac{Y_h}{X_h}\right) + \phi_{\mathrm{dec}}, \tag{25}$$

where ϕ_{dec} is the earth magnetic declination angle at a given point on the earth surface, as shown in Fig. 3. The detail derivation of equation (23), (24) and (25) is given in [25].

In the complementary Kalman filter the integration of the Euler angles is performed outside of the Kalman filter. This structure requires a much lower sampling rate and guarantees that the rapid dynamic response of the inertial system will not be compromised by the Kalman filter [8].

The state-estimate vector $\mathbf{x}_{6\times1}$ for Kalman filter is set as $[\delta\Theta,\ \delta\Omega]^T$, $\delta\Theta$ stands for orientation error of three Euler angles and $\delta\Omega$ presents the angular rate error or gyro bias in **b**-frame. The measurement $\mathbf{y}_{3\times1}$ is set as the difference between two sets of orientation data $[\Theta^{\mathrm{R}} - \Theta]^T$. The detail of the filter structure and the derivation of the filter can be found in [6]. Since the reference orientation is calculated on condition that the IMU is in static case, Θ^{R} will be fused with

Θ only when the value of $\|a\| = \sqrt{a_{b,x}^2 + a_{b,y}^2 + a_{b,z}^2}$ is close to gravity g. Besides, it is important to mention that the non-bias error terms of the filter state estimate $\mathbf{x}_{6\times1}$: $\delta\Theta$ needs to be reset to zero after correcting the current orientation and the gyro bias $\delta\Omega$ will be maintained over time.

B. Magnetic Disturbances Detection and Minimization

The idea of magnetic field disturbances detection and minimization is that if magnetic field disturbances are detected, the date fusion procedures will not depend on magnetic field sensor. Since the magnetic field vector is always involved in determination of ψ^{R}, an alternative vector, which is not affected by magnetic field disturbances, needs to be obtained.

The following content is to improve and extend our previous work [17]. Based on [27] it was assumed that the earth magnetic field is parallel with respect to the earth surface for simplification. However, in order to enhance the accuracy of the estimation of the magnetic field vector in **e**-frame, the inclination angle needs to be considered, since the Earth's magnetic lines of force generally are not parallel to the surface. According to [16], the expected earth magnetic field vector referenced to **n**-frame can be set as

$$\mathbf{M}_n^{\mathrm{R}} = [\mathrm{M}\cdot\sin(\phi_{\mathrm{inc}}),\ 0,\ \mathrm{M}\cdot\cos(\phi_{\mathrm{inc}})]^T. \tag{26}$$

M denotes the earth magnetic field magnitude in the region of interest. If there is no magnetic field disturbances, normalized value of M should be 1. Since we are considering the disturbance-free case for magnetic field correction, M is always set as 1. ϕ_{inc} is the earth magnetic inclination angle at a given point on the earth surface. Therefore, if **DCM** is known, the reference earth magnetic field vector in the **b**-frame $\mathbf{M}_b^{\mathrm{R}}$ can be calculated by

$$\mathbf{M}_b^{\mathrm{R}} = \mathbf{DCM}^{-1}\cdot\mathbf{M}_n^{\mathrm{R}}. \tag{27}$$

If the magnetic field sensor is experiencing magnetic field disturbances, $\mathbf{M}_b^{\mathrm{R}}$ is used to determine the reference yaw angle instead of $\mathbf{M}_b$.

According to [9], $\|m\| = \sqrt{m_{b,x}^2 + m_{b,y}^2 + m_{b,z}^2} = 1$ and dip angle $\phi_{\mathrm{mag}} = \arctan(\frac{m_{n,z}}{m_{n,x}^2+m_{n,x}^2})$ at each time step are used to tell whether or not the magnetic field is disturbed. And $\mathbf{M}_n = [m_{n,x},\ m_{n,y},\ m_{n,z}]^T = \mathbf{DCM}\cdot\mathbf{M}_b$. However, we found that detection based only on this criterion was not sufficient. Sometimes, even if $\|m\|$ and ϕ_{mag} are close to 1 and the local inclination angle[2], the sensor still suffers from the disturbances. Thereby, additional criterion for detection must be applied.

The magnetic field disturbances detection procedures are shown as follows:

1) Firstly at each time point $\|m_k\|$ and $\phi_{\mathrm{mag},k}$ must fulfill the tolerance range around 1 and local inclination angle.
2) Secondly, under the assumption that there is no magnetic field disturbances, multiplying $\mathbf{A}_b^T$ by $\mathbf{M}_b$ results a constant value during the whole time period [28].

$$C = \mathbf{A}_b^T\cdot\mathbf{M}_b. \tag{28}$$

[2]http://magnetic-declination.com/

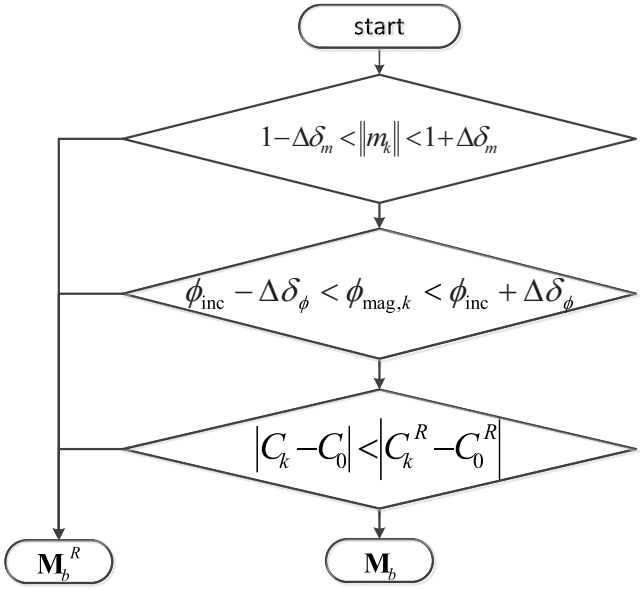

Fig. 4. Magnetic field disturbances detection flow chart.

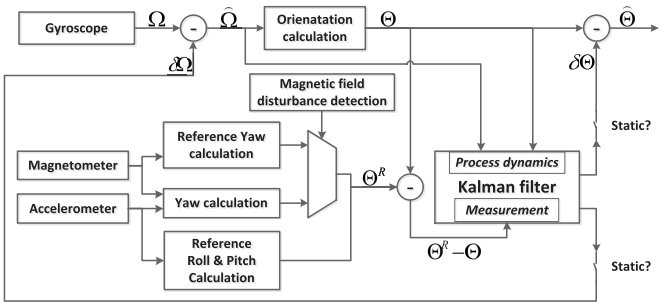

Fig. 5. Structure of modified Kalman filter.

C_k and C_k^{R} are defined as the constant values of time step k calculated by $\mathbf{M}_b$ and $\mathbf{M}_b^{\mathrm{R}}$. Although the gyro based orientation suffers from sensor drift, error is accumulated slowly during the time. To the opposite, reference orientation Θ^{R} calculated by (21), (22) and (25) shows some rapid-changed ripples when magnetic field is disturbed. Therefore, if $|C_k - C_0|$ is smaller than $|C_k^{\mathrm{R}} - C_0^{\mathrm{R}}|$, which means the variation of $\mathbf{M}_b$ is smaller than $\mathbf{M}_b^{\mathrm{R}}$, $\mathbf{M}_b$ is assumed undisturbed and usable.

Note that $\mathbf{M}_b$ can be used only if both criterions are fulfilled. The detection flow-chart is shown in Fig. 4. The structure of modified Kalman filter is depicted in Fig. 5.

The following results show how the magnetic field disturbances detection and minimization improve the reference yaw angle ψ^{R}. The result is based on the outdoor experiment studied in [17], since the improvement can be seen distinctly with less magnetic field disturbances and a approximative constant velocity.

Fig. 6 shows how $\|m\|$ and $\phi_{\mathrm{mag},k}$ changed during the experiment comparing with the ideal ones, which was 1 and -1.114 rad. We can see that despite being in outdoor environment the magnetic field was still affected by ferromagnetic materials.

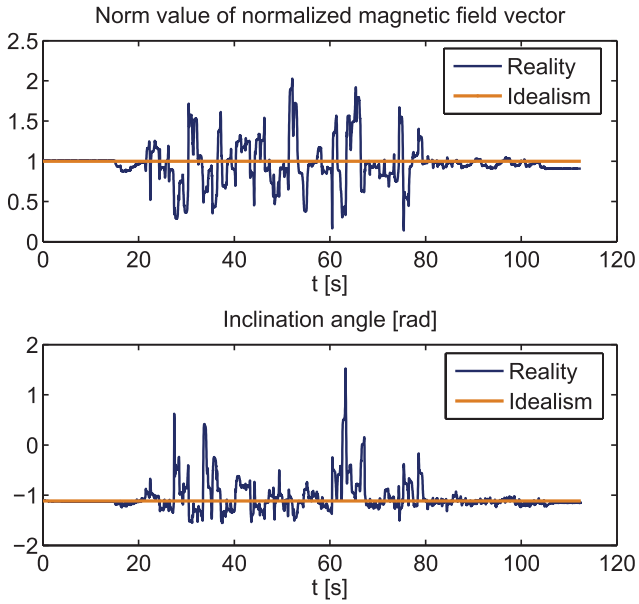

Fig. 6. Magnetic field disturbances detection.

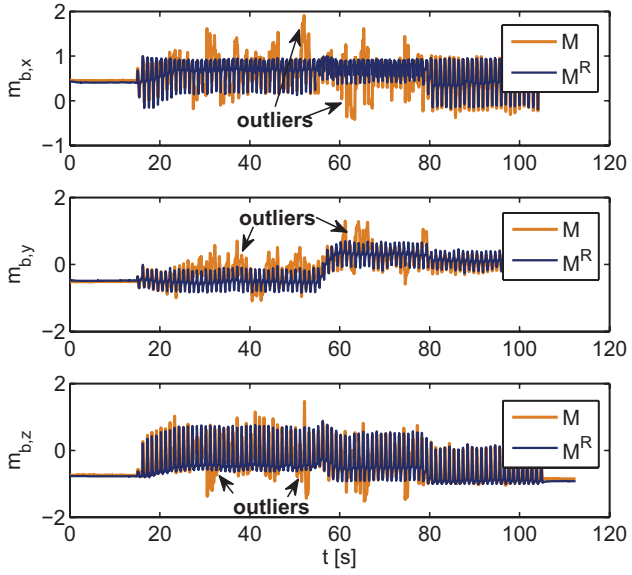

Fig. 7. Comparison of sensed and reference magnetic field vectors.

Fig. 7 shows that $\mathbf{M}_b^{\mathrm{R}}$ is much more stable and robust than $\mathbf{M}_b$. since there is no outliers existing and the outline of the data set is smoother, i.e. $\mathbf{M}_b^{\mathrm{R}}$ is able to follow the change of yaw angle.

As shown in Fig. 8, after the correction the influence of magnetic field disturbances can be efficiently removed. The tendency of resulted ψ^{R} is also similar to ψ. More information of this outdoor experiment can be found in [17].

III. Position and Velocity Correction

Generally, the position information can be determined if the step length, direction and number of steps are obtained. The step boundaries can be defined by the positive-going zero crossings of a low-pass filtered version of acceleration signal [29]. And the performance of this system mainly depends

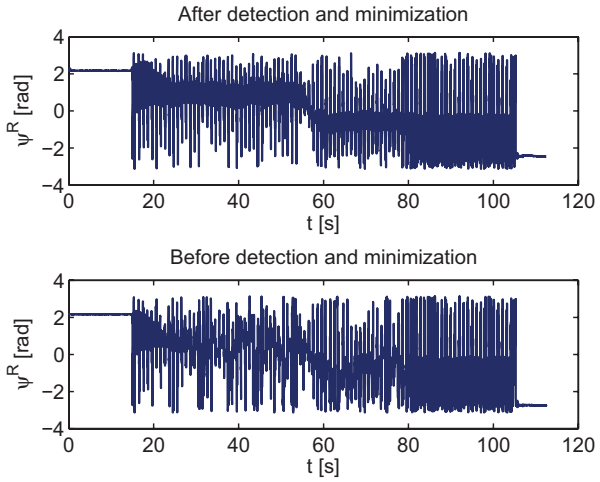

Fig. 8. Reference yaw ψ^{R} before and after correction.

on the accuracy of step length determination, which can be obtained by GPS or artificial neural network [29], [30]. However, constant step length condition may not always be met, since emergency responders may run, climb over debris, or may alter their step length as a function of the weight of their gear.

In the whole phase of a stride during normal walking, there exists a time period when the foot is not moving relative to the ground. This time period is called sill phase. Ojeda and Borenstein showed that the velocity value should be reset when still phase is detected, thus the accumulated errors from the accelerometer output could be effectively removed [18]. This method is called "Zero Velocity Update" (ZUPT). The accuracy of the ZUPT based solution relies on the accuracy of still phase detection.

Experimentally the best indication for still phase could be obtained by observing the three outputs of gyroscopes. If the norm value of gyroscopes' outputs is smaller than the predefined threshold, we assume that the foot is within still phase and the velocity can be reset.

$$\|\omega_k\| = \sqrt{\omega_{x,k}^2 + \omega_{y,k}^2 + \omega_{z,k}^2}. \tag{29}$$

$$\begin{cases} \|\omega_k\| \le \delta, & \text{still} \\ \text{others}, & \text{swing}, \end{cases} \tag{30}$$

where $\omega_{x,k}$, $\omega_{y,k}$ and $\omega_{z,k}$ are the angular rates of three orthogonal axes in **b**-frame at time step k, δ is the predefined threshold for ZUPT still phase detection.

Assume $v_{x,k}$ to be the linear velocity values at time step k of the x-axis in **b**-frame which have to be corrected. The resetting procedures are given as follows:

1) Let k_{start} be the moment when the still phase starts, and $v_{x,k_{\mathrm{start}}}$ will be the value of the velocity at this moment. k_{end} will be the moment in which the still phase ends and the next step starts, with its velocity value $v_{x,k_{\mathrm{end}}}$.
2) The mean velocity value u during the still phase is computed by

$$u = \frac{1}{k_{\mathrm{end}} - k_{\mathrm{start}}} \sum_{k=k_{\mathrm{start}}}^{k_{\mathrm{end}}} v_{x,k}. \tag{31}$$

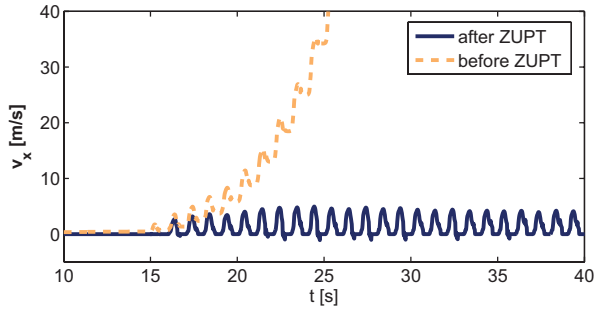

Fig. 9. Comparison of ZUPT applied and not applied velocities [20].

3) The linear velocity values are corrected according to the following equation

$$v'_{x,k} = v_{x,k} - u|_{k=k_{\text{start}}\ldots k_{\text{end}}}. \tag{32}$$

The same procedures apply for v_y and v_z. After implementing ZUPT method, the boundless-increased velocity error is efficiently removed as shown in Fig. 9.

IV. Human Body Movement Monitoring

In order to track the full-body human motion, in this study the human body is considered as 14 rigid segments as shown in Fig. 10. IMU is mounted on the center of each segment to obtain segment's inertial, magnetic field and orientation information.

Define $\mathbf{ROT}_i^{i+1}$ as the rotation matrix which transforms the **b**-frame coordinate of segment $i+1$ to **b**-frame coordinate of segment i. The rotation matrix can be calculated either by gravity or magnetic field vector in **b**-frame according to [23]. Since magnetic field could be disturbed by ferromagnetic material, gravity is selected rather then magnetic field as shown below.

$$[g_x^{i+1},\ g_y^{i+1},\ g_z^{i+1}]^T = \mathbf{ROT}_i^{i+1} \cdot [g_x^i,\ g_y^i,\ g_z^i]^T, \tag{33}$$

where $[g_x^i,\ g_y^i,\ g_z^i]^T$ denotes the gravity components in **b**-frame $\mathbf{G}_b^i$ measured by IMU attached to the segment i. However $\mathbf{G}_b$ can not be easily obtained due to the fact that the output of the acceleration sensor contains the gravity components and acceleration of movement. If the large-range movement is made, the obtained $\mathbf{ROT}_i^{i+1}$ based on (33) will not be correct as well. Since $\mathbf{G}_b$ can be calculated by **DCM** and gravity vector in **n**-frame $[0,\ 0,\ g]^T$, (33) can be rewritten as

$$\mathbf{ROT}_i^{i+1} = \mathbf{DCM}_{i+1} \cdot \mathbf{DCM}_i^T, \tag{34}$$

where $\mathbf{DCM}_i$ stands for the Direction Cosine Matrix of segment i. A local transfer matrix $\mathbf{Trans}_i^{i+1}$ consisting of the segment's rotation and displacement information is given as follows:

$$\mathbf{Trans}_i^{i+1} = \begin{bmatrix} & & & 0 \\ & \mathbf{ROT}_i^{i+1} & & W_i \\ & & & l_i \\ 0 & 0 & 0 & 1 \end{bmatrix}, \tag{35}$$

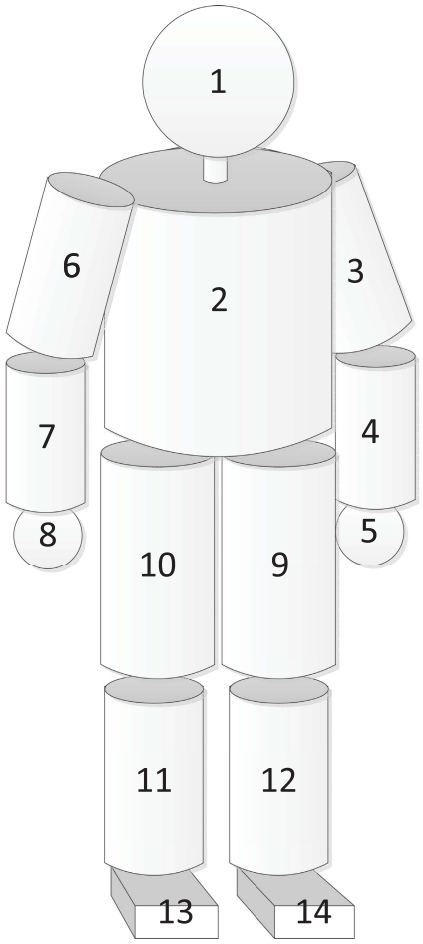

Fig. 10. Depiction of the 14 segments comprising stick figure for human body.

where W_i and l_i denote the physical length and width of the segment i. $\mathbf{Trans}_i^i$ is given as

$$\mathbf{Trans}_i^i = \begin{bmatrix} & & & 0 \\ & \mathbf{I}_3 & & W_i \\ & & & l_i \\ 0 & 0 & 0 & 1 \end{bmatrix}, \tag{36}$$

where $\mathbf{I}_3$ is 3-by-3 identity matrix. In order to calculate the relative position of the segment i with respect to the coordinate frame of reference segment j, a global transfer matrix $\mathbf{TransG}_j^i$ from segment i to reference segment j is obtained as in equation 37.

$$\begin{aligned} \mathbf{TransG}_j^i &= \mathbf{Trans}_j^{j+1} \cdots \mathbf{Trans}_{i-1}^i \cdot \mathbf{Trans}_i^i \\ &= \begin{bmatrix} r_{11} & r_{12} & r_{13} & p_x \\ r_{21} & r_{22} & r_{23} & p_y \\ r_{31} & r_{32} & r_{33} & p_z \\ 0 & 0 & 0 & 1 \end{bmatrix}^T, \end{aligned} \tag{37}$$

where $[p_x,\ p_y,\ p_z]^T$ is the vector of relative position of segment i respect to the coordinate system of segment j. Other terms of $\mathbf{TransG}_j^i$ indicate the multiplication result of rotation matrices.

Fig. 11. Environment inside the building.

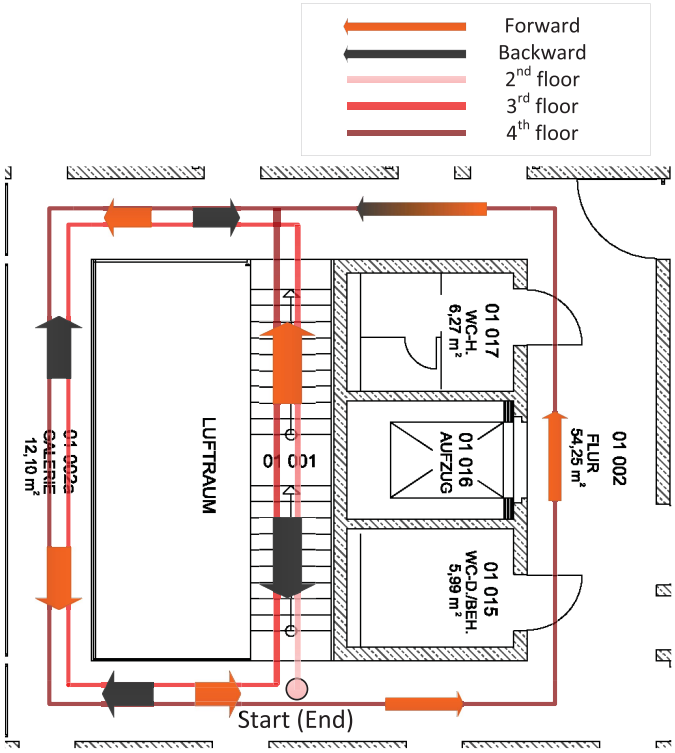

Fig. 12. Plain map of the building.

V. Numerical Study

The purpose of the experiments was to investigate the capability and accuracy of indoor localization system. For the experiments, six IMUs produced by the company *Xsens*[3] were used. The IMUs were attached on the human segments 9−13 and segment 2 based on Fig. 10. The IMU consists of 3 gyroscopes, 3 accelerometers, 3 magnetic field sensors, and a temperature sensor for 3D measurement. The usage range of accelerometer and gyroscope are limited to $\pm 5g$ m^2/s and ± 1200 deg/s respectively. In this study all sensor signals were sampled at 50 Hz.

IMUs from segment 9-12 and segment 2 are used to monitor the movement of human body. IMU from segment 13 is used to calculate the position and its corresponding velocity by applying modified Kalman filtering and ZUPT method.

[3]www.xsens.com

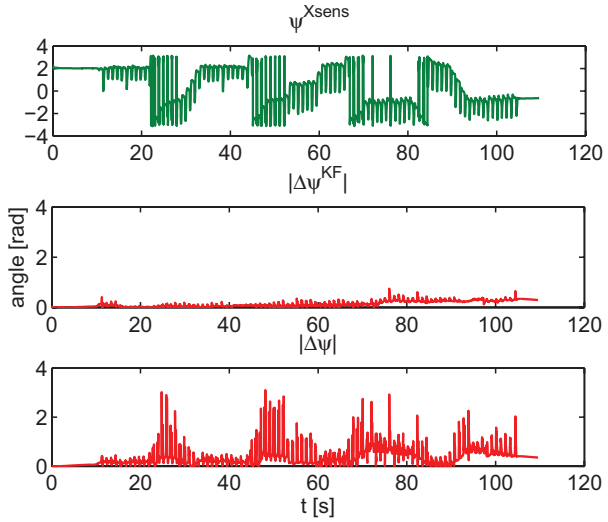

Fig. 13. Yaw angle differences between the Xsens's output ψ^{Xsens}, Kalman filtered ψ^{KF} gyro-based ψ when stairs climbing at speed of walking.

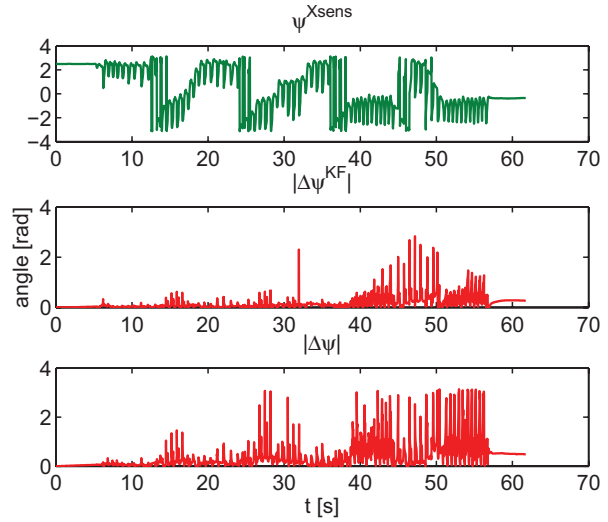

Fig. 14. Yaw angle differences between the Xsens's output ψ^{Xsens}, Kalman filtered ψ^{KF} gyro-based ψ when stairs climbing at speed of running.

The experiments were held inside a building starting on the 2$^{\text{nd}}$ floor shown in Fig. 11. The person mounted with IMUs walked/ran firstly upstairs to the 4$^{\text{th}}$ floor, then walked/ran around the 4$^{\text{th}}$ floor, and later came back to the 2$^{\text{nd}}$ floor, as shown in Fig. 12. Notice that the ferromagnetic materials inside the building, such as iron stairs handle and office door, did strongly affect the measurement of the magnetic field sensor. For human body monitoring, the segment 2 was set as the reference segment. It is necessary to mention that IMU from segment 2 is also used to classify and recognize human activities at different speed, i.e. running or walking, since a modified ZUPT method instead of normal one was applied in this study to obtain proper ZUPT threshold for high-speed movement. The detail of modified ZUPT method can be found in [20].

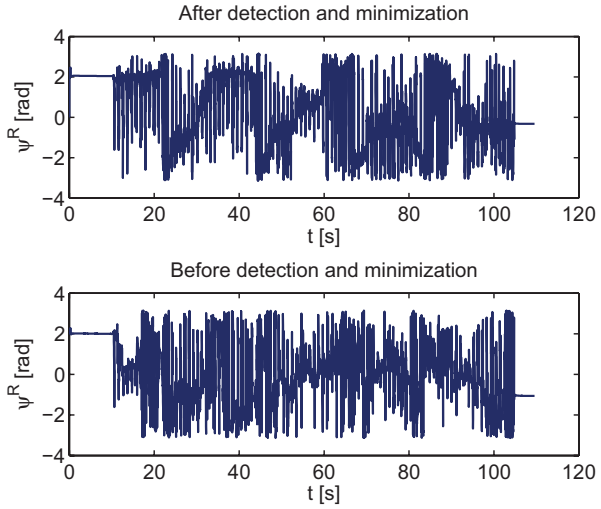

Fig. 15. Reference yaw ψ^{R} before and after correction when stairs climbing at speed of walking.

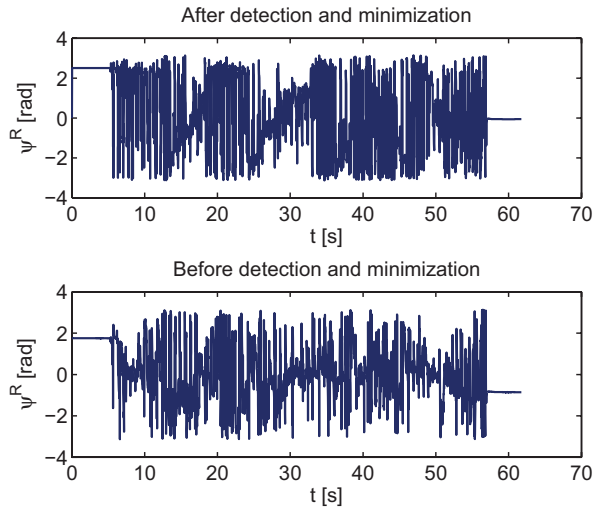

Fig. 16. Reference yaw ψ^{R} before and after correction when stairs climbing at speed of running.

TABLE I
MEAN OVER TIME OF RMSE

[rad]	Roll	Pitch	Yaw
Stairs climbing at speed of walking	0.11	0.05	0.17
Stairs climbing at speed of running	0.35	0.11	0.32

A. Orientation Determination Overcoming Magnetic Field Disturbances

The comparison of yaw angle data sets of both experiment scenarios are shown in Fig. 13 and Fig. 14. $|\Delta\psi^{\mathrm{KF}}|$ is the absolute angle difference between the Xsens's output ψ^{Xsens} and ψ^{KF} which is fused by gyro based yaw ψ and corrected reference yaw ψ^{R}. $|\Delta\psi|$ is the absolute angle difference between ψ^{Xsens} and ψ. It can be seen that $|\Delta\psi^{\mathrm{KF}}|$ is much smaller than $|\Delta\psi|$, which means that the accumulated drift error has been efficiently removed by Kalman filtering based data fusion.

The performance of ψ^{KF} benefited a lot from corrected ψ^{R}, which maintained the correct outline of magnetic field based orientation and removed the noise outliers, as shown in Fig. 15 and 16. Table I shows the mean over time of root mean square error (RMSE) comparing with Xsens's output.

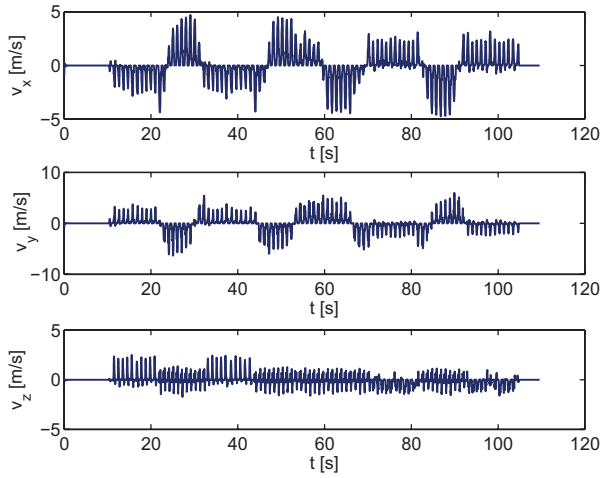

Fig. 17. Velocities of three axes in **e**-frame.

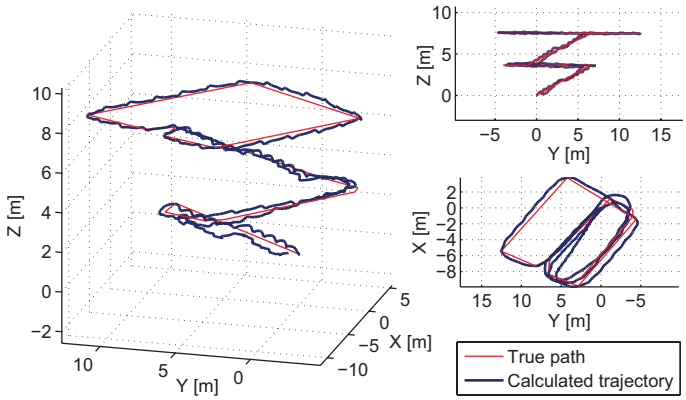

Fig. 18. Trajectory of stairs climbing at speed of walking.

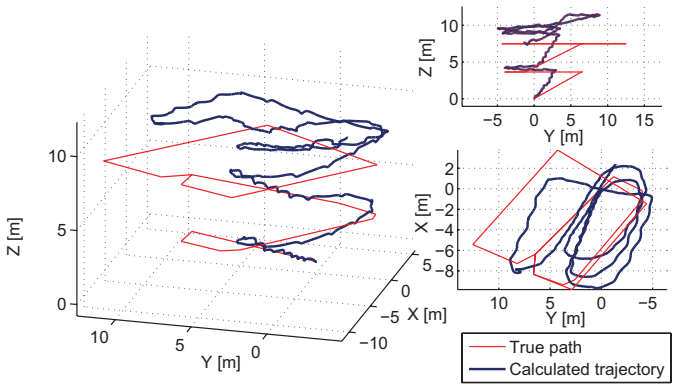

Fig. 19. Trajectory of stairs climbing at running speed.

B. Velocity and Position Correction by ZUPT

1) Stairs Climbing at Speed of Walking: Fig. 17 shows the velocity changes in **n**-frame during the experiment. After detecting the correct still phase, the accumulated error can be efficiently removed by ZUPT. The accumulated position error of each axis can be calculated by multiplying the sum

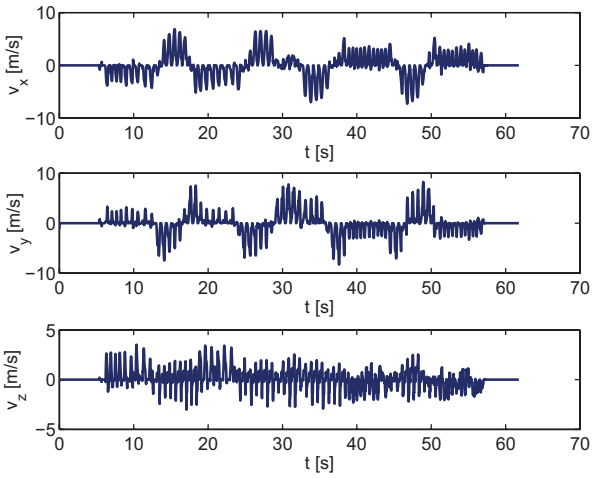

Fig. 20. Velocities of three axes in **e**-frame.

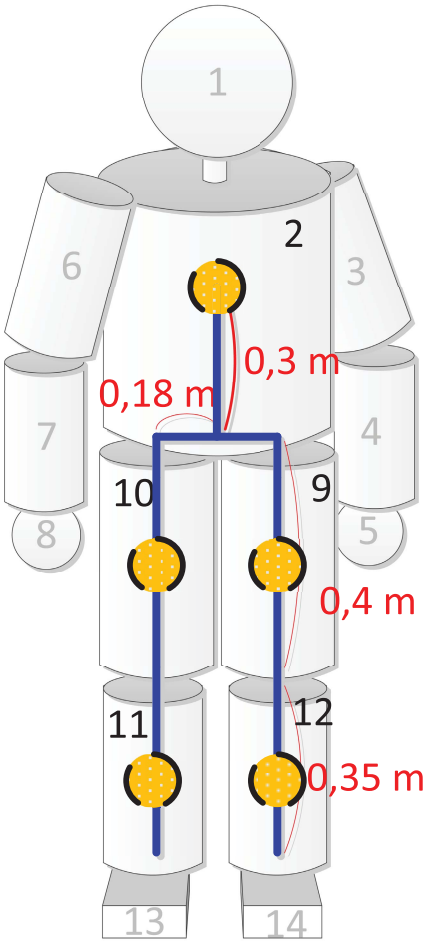

Fig. 21. Body segments used for motion monitoring.

of velocities at each time step by time step duration (0.02 s), since the person mounted with IMUs walked back to the start point. The trajectory in 3D and its partial result in 2D are shown in Fig. 18. It can be seen that the shape of the stairs and corridor can be accurately reformed in both height and planar orientation. The accumulated error in $X-Y-Z$ directions are 0.973 m, -1.11 m, and -0.645 m respectively.

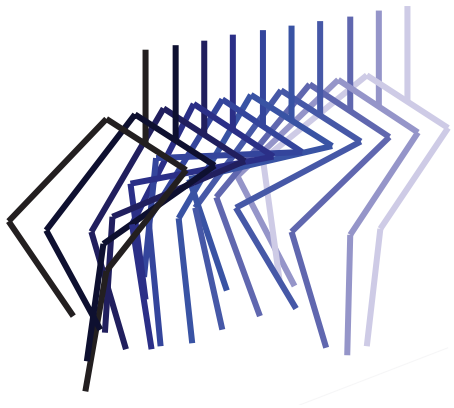

Fig. 22. Motion monitoring of stairs climbing at speed of walking within one step.

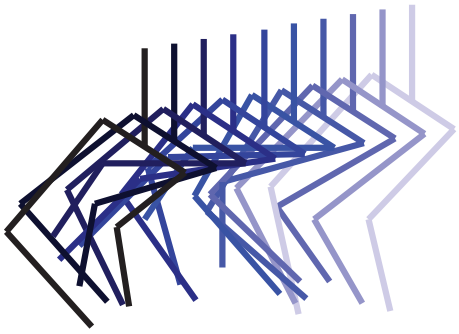

Fig. 23. Motion monitoring of stairs climbing at speed of running within one step.

2) Stairs Climbing at Speed of Running: Fig. 19 shows the trajectory in 3D and 2D from stairs climbing at running speed. Although the 2D plain result shows the path is distorted and declined compared with the one at lower speed, the scalar and outline is similar. However the height information is not correct in this situation. It can seen that the downstairs part shrinks, which means that the calculated velocity during downstairs running in z direction is too small, as can be seen in Fig. 20. The accumulated errors in $X-Y-Z$ directions are 2.35 m, -1.39 m, and 7.73 m. The incorrect height estimation and shifted 2D view direction could be due to the inaccurate orientation information, since the acceleration and angular rate of movement sometimes extend the measurement range of the inertial sensors.

C. Tracking of Human Body Movement

The orientation information from segments 9-12 and segment 2 were used to monitor the human body movements when climbing stairs. The yellow circles stand for IMUs. The physical lengths of these segments are shown in Fig. 21. Fig. 22 and Fig. 23 show how lower part of human body move within one step. We took 1 sample per 5 samples for walking case and 1 sample per 3 samples for running case so as to deliver sufficient information while limiting the number of the figure frames. The color of the body segments gets darker as the time passes.

VI. Conclusion

This paper presented a new localization system based on inertial sensors for emergency responders. The IMUs were attached on different segments of human body for different uses. The foot-mounted IMU was used to obtain the correct orientation information by using modified Kalman filter, which overcame the impact of the magnetic field disturbances, then calculate the correct velocity and position information of emergency responders using the determined orientation and ZUPT method. Meanwhile all IMUs were used to monitor the behavior of each segment of human body by processing the orientation information of each human body segment, thus the relative position of each segment could be achieved.

The experimental results showed that the system was able to deliver correct 3D position information in both walking and running cases. In the meantime, the correct real-time segment monitoring was also achieved. However, since the system is calculated recursively, the error is always accumulated with time. We can image that the trajectory will certainly be biased after several repetitions. The system for long term accurate tracking eventually needs the aid of absolute position reference, which can be obtained by network infrastructure based localization [3]. The future work is to combine both systems to yield on the one hand, a minimized influence of obstacles by inertial sensor based tracking and on the other hand, a reduction of accumulated errors by resetting the initial position obtained by infrastructure based localization.

References

[1] C. Fischer and H. Gellersen, "Location and navigation support for emergency responders: A survey," *IEEE Pervas. Comput.*, vol. 9, no. 1, pp. 38–47, Jan.–Mar. 2010.

[2] R. Zhang, "Wireless network-based positioning of a mobile station in non-line-of-sight environment," M.S. thesis, Dept. Comput. Sci., Darmstadt Univ. Technology, Darmstadt, Germany, 2009.

[3] R. Zhang, F. Höflinger, and L. M. Reindl, "TDOA based localization using interacting multiple model estimator and ultrasonic transmitter/receiver," in *Proc. 9th Int. Multiconf. Syst., Signals Device*, 2012, pp. 1–6.

[4] M. Sippel, "Localization of mobile objects with embedded microsystems," Ph.D. dissertation, Dept. Electr. Eng., Albert-Ludwigs-Univ. Freiburg, Freiburg, Germany, 2010.

[5] J. Müller, "Techniken für die navigation autonomer luftschiffe," M.S. thesis, Dept. Comput. Sci., Univ. Freiburg, Freiburg, Germany, 2008.

[6] E. Foxlin, "Inertial head-tracker sensor fusion by a complementary separate-bias Kalman filter," in *Proc. Virtual Real. Annu. Int. Symp.*, 1996, pp. 185–194.

[7] S. Han and J. Wang. (2009). *A Novel Method to Integrate IMU and Magnetometers in Attitude and Heading Reference Systems* [Online]. Available: http://www.gmat.unsw.edu.au/snap/publications/hans&wang_2009a.pdf

[8] P. Setoodeh, A. Khayatian, and E. Farjah, "Attitude estimation by separate-bias Kalman filter-based data fusion," *J. Navigat.*, vol. 57, no. 2, pp. 261–273, 2004.

[9] D. Roetenberg, H. J. Luinge, C. T. B. Baten, and P. H. Veltink, "Compensation of magnetic disturbances improves inertial and magnetic sensing of human body segment orientation," *IEEE Trans. Neural Syst. Rehabil. Eng.*, vol. 13, no. 3, pp. 395–405, Sep. 2005.

[10] H. J. Luinge, "Inertial sensing of human movement," Ph.D. dissertation, Inst. Biomed. Technol., Univ. Twente, Enschede, The Netherlands, 2002.

[11] H. J. Luinge, P. H. Veltink, and C. T. Baten, "Estimating orientation with movement using a 3-D accelerometer with autocalibration," *IEEE Trans. Neural Syst. Rehabil. Eng.*, vol. 12, no. 1, pp. 112–121, Mar. 2004.

[12] E. Foxlin, "Pedestrian tracking with shoe-mounted inertial sensors," *IEEE Comput. Graph. Appl.*, vol. 25, no. 6, pp. 38–46, Nov.–Dec. 2005.

[13] A. R. Jiménez, F. Seco, J. C. Prieto, and J. Guevara, "Indoor pedestrian navigation using an INS/EKF framework for yaw drift reduction and a foot-mounted IMU," in *Proc. 7th Workshop Position. Navigat. Commun.*, 2010, pp. 135–143.

[14] A. R. Jiménez, F. Seco, J. C. Prieto, and J. Guevara, "Accurate pedestrian indoor navigation by tightly coupling foot-mounted IMU and RFID measurements," *IEEE Trans. Instrum. Meas.*, vol. 61, no. 1, pp. 178–189, Jan. 2012.

[15] J. Calusdian, X. Yun, and E. R. Bachmann, "Adaptive-gain complementary filter of inertial and magnetic data for orientation estimation," in *Proc. IEEE Int. Conf. Robot. Autom.*, Mar. 2011, pp. 1916–1922.

[16] X. Yun, J. Calusdian, E. R. Bachmann, and R. B. McGhee, "Estimation of human foot motion during normal walking using inertial and magnetic sensor measurements," *IEEE Trans. Instrum. Meas.*, vol. 61, no. 7, pp. 1–14, Jul. 2012.

[17] R. Zhang and L. M. Reindl, "Pedestrian motion based inertial sensor fusion by a modified complementary separate bias Kalman filter," in *Proc. IEEE Sensors Appl. Symp.*, Feb. 2011, pp. 209–213.

[18] L. Ojeda and J. Borenstein, "Non-GPS navigation for security personnel and first responders," *J. Navigat.*, vol. 60, no. 3, pp. 391–407, 2007

[19] L. Ojeda and J. Borenstein, "Personal dead-reckoning system for GPS-denied environments," in *Proc. IEEE Int. Workshop Safety Security Rescue Robot.*, Sep. 2007, pp. 1–6.

[20] R. Zhang, M. Loschonsky, and L. M. Reindl, "Study of zero velocity update for both low- and high-speed human activities," *Int. J. E-Health Med. Commun.*, vol. 2, no. 2, pp. 46–67, 2011.

[21] V. Renaudin, O. Yalak, P. Tomé, and B. Merminod, "Indoor navigation of emergency agents," *Eur. J. Navigat.*, vol. 5, no. 3, pp. 36–45, 2007.

[22] H. Zhou and H. Hu, "Reducing drifts in the inertial measurements of wrist and elbow positions," *IEEE Trans. Instrum. Meas.*, vol. 59, no. 3, pp. 517–585, Mar. 2010.

[23] R. Zhu and Z. Zhou, "A real-time articulated human motion tracking using tri-axis inertial/magnetic sensors package," *IEEE Trans. Neural Syst. Rehabil. Eng.*, vol. 12, no. 2, pp. 295–302, Jun. 2004.

[24] K. N. Vikas, "Integration of inertial navigation system and global positioning system using Kalman filtering," Ph.D. dissertation, Dept. Aerosp. Eng., Indian Inst. Technology, Bombay, India, 2004.

[25] M. J. Caruso, "Applications of magnetic sensors for low cost compass systems," in *Proc. IEEE Position Locat. Navigat. Symp.*, San Diego, CA, Mar. 2000, pp. 177–184.

[26] W. Benenson, J. W. Harris, H. Stocker, and H. Lutz, *Handbook of Physics*. New York: Springer-Verlag, 2002.

[27] J. Torres, B. O'Flynn, P. Angove, F. Murphy, and C. O'Mathuna, "Motion tracking algorithms for inertial measurement," in *Proc. 2nd ICST Int. Conf. Body Area Netw.*, 2007, pp. 1–18.

[28] R. B. Smith, B. G. Morton, and M. R. Elgersma, "Electronic compass and compensation of large magnetic errors for operation over all orientations," U.S. Patent 6 543 146, Apr. 8, 2003.

[29] S. Beauregard and H. Haas, "Pedestrian dead reckoning: A basis for personal positioning," in *Proc. 3rd Workshop Position., Navigat. Commun.*, 2006, pp. 27–35.

[30] S. Y. Cho and C. G. Park, "MEMS based pedestrian navigation system," *J. Navigat.*, vol. 59, no. 1, pp. 135–153, 2006.

Rui Zhang received the B.Sc. degree from the Beijing University of Aeronautics and Astronautics, Beijing, China, and the M. Sc degree from the Institute of Telecommunications, Darmstadt University of Technology, Darmstadt, Germany, in 2006 and 2009, respectively. He is currently pursuing the Ph.D. degree focusing on indoor localization technologies with the Laboratory for Electrical Instrumentation, Institute of Microsystem Technology, Albert-Ludwigs University of Freiburg, Germany.

His current research interests include wireless infrastructure-based localization, inertial sensor-based localization, human movement monitoring, and classification.

Mr. Zhang was a recipient of the Siemens Master Program Scholarship for the Master study in Germany in 2006.

Fabian Höflinger received the B.Sc. degree in automation engineering from the University of Applied Sciences, Friedrichshafen, Germany, and the Master's degree in automation and energy systems from the University of Applied Sciences, Mannheim, Germany, in 2007. He is currently pursuing the Ph.D. degree focusing on indoor-localization systems with the Laboratory for Electrical Instrumentation, Institute of Microsystem Technology, Albert-Ludwigs University of Freiburg, Freiburg, Germany.

He was with Junghans Feinwerktechnik, Schramberg, Germany, during his Bachelor's studies, where he had developed components for telemetric systems. He developed inductive electronic components for programmable fuses during his Master's studies. From 2007 to 2010, he was with a Company of telemetric systems, where he involved in inductive measurement and signal transformation.

Leonhard Reindl received the Diploma degree in physics from Technische Universität München, Munich, Germany, and the Dr. sc. techn. degree from the Vienna University of Technology, Vienna, Austria, in 1985 and 1997, respectively.

He joined the Surface Acoustic Wave Department, Siemens Corporate Technology Division, Munich, Germany, in 1985, where he was engaged in the development of surface acoustic wave (SAW) devices for signal processing and matched filtering in radio communications, radar systems, SAW-based identification marks, and wireless passive SAW-based sensors. In 1999, he joined the Institute of Electrical Information Technology, Clausthal University of Technology, Clausthal-Zellerfeld, Germany. In 2003, he joined as a Full Professor of electrical instrumentation with the Institute for Microsystem Technology, Albert-Ludwigs University of Freiburg, Freiburg, Germany. He has authored or co-authored more than 250 papers on SAW devices and wireless passive sensor systems and holds 45 patents. His current research interests include wireless sensor systems, energy-harvesting systems, local positioning systems, and search and rescue systems for people buried in disasters.

Dr. Reindl is a member of the Technical Program Commitees of the IEEE Frequency Control Symposium, the IEEE Ultrasonic Symposium, Eurosensors, Sensors, and the German Biannual Symposium "Sensoren und Messsysteme." He was and is an Elected Member of the AdCom of the IEEE UFFC Society from 2005 to 2007 and from 2010 to 2012.